

Original Research

Natural Soil Clays from a Phaeozem to Synthesize a Nanocomposite with Exhausted Coffee Grounds and Ag- and TiO₂-Nanoparticles for Water, Air, or Soil Decontamination

Vianey Urdapilleta-Inchaurregui¹, Fabián Fernández-Luqueño^{2*},
Aidé Minerva Torres-Huerta³, Daniela Roa-Velázquez¹,
Francisco Javier Rodríguez-Varela², María Esther Sánchez-Castro²

¹Programa de Nanociencias y Nanotecnología, Cinvestav, Av. Instituto Politécnico Nacional 2508, Ciudad de México, 07000, México

²Sustainability of Natural Resources and Energy Programs, Cinvestav-Salttillo, Av. Industria Metalúrgica 1062, Parque Industrial Saltillo-Ramos Arizpe, Ramos Arizpe, Coahuila, 25900, Mexico

³Instituto Politécnico Nacional, CICATA-Altamira, km 14.5 Carr. Tampico-Pto. Ind. Altamira, Altamira, Tams. México, 89600, Mexico

Received: 27 January 2020

Accepted: 14 April 2020

Abstract

A nanocomposite using natural clays from a Phaeozem soil, engineered Ag-nanoparticles (NP), TiO₂-NP, and exhausted coffee grounds was synthesized through a single-step by thermal method, to degrade or filtrate pollutants from soils, water or air. The surface characteristics and the porosity of the composite were studied through nitrogen gas adsorption and application of the Brunauer-Emmett-Teller (BET) equation, and the microporous composites ranged a surface area of 17.36 m² g⁻¹. X-ray diffraction showed the crystalline structure and crystalline phase of the nanocomposites. High-resolution transmission electron microscopy (HR-TEM) and scanning transmission electron microscopy (STEM) demonstrated that TiO₂-NP surrounded Ag-NP, and both were impregnated on natural soil NP. Oxidation states of the Ag-NP and TiO₂-NP were analyzed by X-ray photoelectron spectroscopy (XPS). The energy gap of nanocomposite 8NC was determined by Ultraviolet-visible diffuse reflectance (UV-Visible DRS). The photocatalytic activity of this nanocomposite was evaluated. The results indicated that nanocomposite with Phaeozem-soil-NP (8NC) degraded 82.31% of the harmful organic compound methylene blue (MB) by 150 minutes, while the antimicrobial activity and resistance against *Escherichia coli* and *Staphylococcus aureus* and the zone of inhibition (ZOI) were 15 mm. The nanocomposite Ag-NP/TiO₂-NP/natural-soil-NP/exhausted

coffee-ground showed its potential for the development of an efficient material for environmental remediation with photocatalytic and antimicrobial activity.

Keywords: environmental pollution and remediation, nanoremediation, photodegradation, water treatment, human and environmental health

Introduction

Emerging contaminants (ECs), along with organic matter and microbes, are the primary source of water pollution [1]. Therefore, novel techniques are required to dissipate or separate the pollutants or microorganisms from drinking water to reduce the increasing hazard regarding illness as a result of drink polluted water. There are different techniques of removal to dissipate contaminants such as coagulation-flocculation, activated carbon adsorption (ACs), ozonation, advanced oxidation processes (AOPs), membrane processes, and membrane bioreactor [2]. Besides, several treatment methods such as biological process, adsorption, catalysis, ozonation, and electrochemical have been applied for the removal of dyes from contaminated water [3]. Among these methods, adsorption is a superior method due to its simplicity of operation, low-cost, fast, highly efficient, and ecofriendly in nature [4].

Some nanoparticles (NP), such as TiO_2 -NP, Ag-NP, or soil clays, have been used in environmental decontamination. One strategy for water purification involves photocatalysts with semiconducting properties such as TiO_2 . Therefore, TiO_2 -NP have been studied in the field of photocatalysis, but these metal oxide can be excited only under UV light irradiation due to their bandgap [5].

It has been reported that a larger surface area and higher crystallinity are conducive to benefit the surface photocatalytic reaction and degradation of pollutants. TiO_2 -NP could incorporate noble metal NP with Pd, Pt, or Ag and could perform their efficiency as photocatalysts through the modification in its structure [6]. Besides, the Ag has been known by their antimicrobial properties through history and Ag-NP by their excellent catalytic efficiency because they can facilitate the electron transfer, but Ag-NP could damage the environment. Therefore, the nanocomposite Ag- TiO_2 -NP could enhance the photocatalytic degradation of various organic pollutants [1-6] but without collateral damage to the environment.

Several studies have reported different techniques for the synthesis of Ag- and TiO_2 -NP and their changes of crystalline structure through the chemical modification, while several forms to attach the Ag-NP and TiO_2 -NP into the clay or natural soils have also been reported [7]. The clay minerals advantages over other adsorbents are their relative abundance in nature, cost-effective, and environmental friendliness in their applications. Furthermore, they have large specific surface areas, high porosity, surface charge, and surface functional groups, which qualify them as

useful adsorbent [8]; these features allow them to attach the Ag-NP and TiO_2 -NP into the layers of clays-NP [8]. Therefore, we hypothesize that the combination of TiO_2 , Ag, exhausted coffee ground, and natural soil will be useful for water purification and environmentally friendly.

The objective of this research was to synthesize and evaluate an Ag-NP/ TiO_2 -NP/Phaeozem soil-NP/exhausted coffee-ground nanocomposite by the thermal method using tetrabutyl titanate and silver nitrate as precursors, and natural soil to build composites with enhanced photocatalytic and antimicrobial activities for the environmental decontamination.

Materials and Methods

All chemical reagents were of analytical grade and used as received without any further purification. Silver nitrate (AgNO_3), tetrabutyl titanate (Titanium(IV) butoxide), $\text{Ti}(\text{OCH}_2\text{CH}_2\text{CH}_2\text{CH}_3)_4$, ethanol, and methylene blue were purchased to Sigma Aldrich. Deionized water was used in all experiments. The natural soil (Phaeozem-soil) was sampled in Metepec, 'Estado de México,' while the Vertisol-soil was sampled in Guanajuato, Mexico. The Gram-negative bacteria *Escherichia coli* and Gram-positive bacteria *Staphylococcus aureus* were purchased from the 'Colección Nacional de Cepas Microbianas y Cultivos Celulares del Cinvestav' at Mexico City and used to test the antimicrobial activity of the synthesized composite.

Preparation of Composite of Ag-NP/ TiO_2 -NP/Phaeozem Soil-NP/exhausted Coffee-Ground

The Ag-NP/ TiO_2 -NP/Phaeozem soil-NP/exhausted coffee-ground nanocomposite was processed by a thermal method and calcinated, as described below. The natural-soil clays and exhausted coffee ground were mixed and placed into a flask; then, 950 mL of ethanol were poured under continuous stirring until a suspension was achieved. Later, 6.5 g AgNO_3 and 30 mL tetrabutyl titanate were added in the suspension and stirred during two h. The suspension was placed into a porcelain crucible and heated at 160°C for 24 h in a high-temperature oven. The suspension was centrifuged at 7800 rpm and washed with deionized water and ethanol to remove impurities. The precipitate was dried at 60°C for two h to obtain black powder. Finally, the powder was calcinated at 500°C , using a temperature ramp of 5°C per minute for twelve hours to

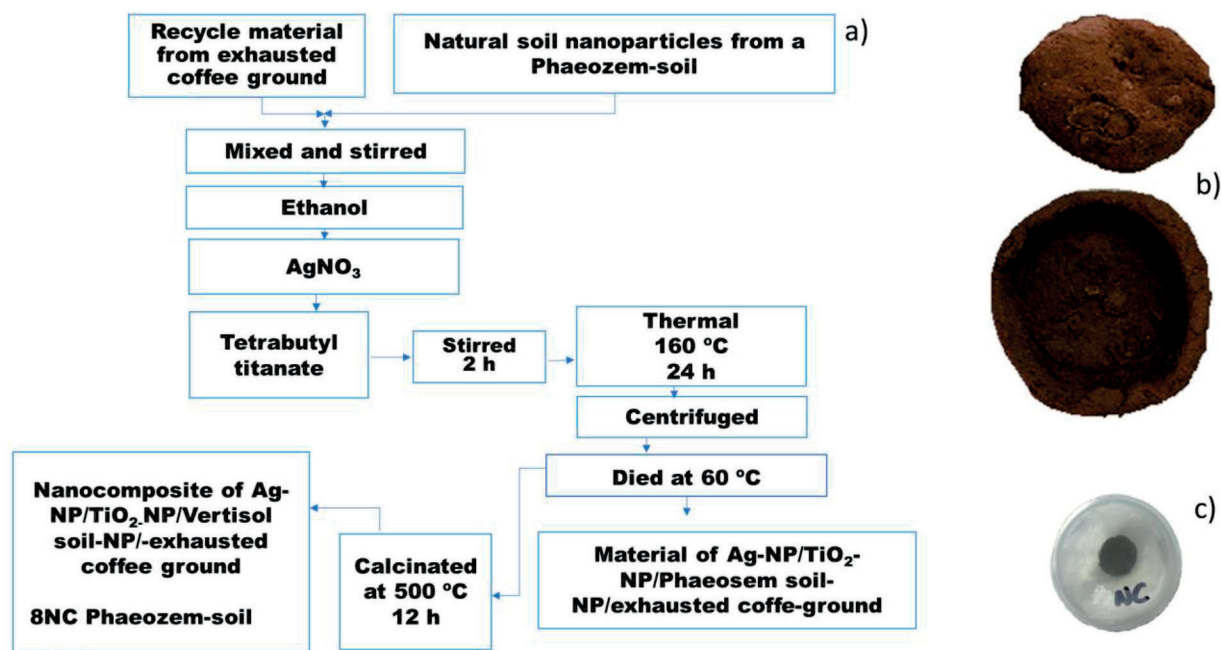


Fig. 1. The synthesis method of the nanocomposite using a Phaeozem soil (8NC), a); photography of the nanocomposite, b); and photography of the tablet produced by scratching the nanocomposite from Fig. b) and then compressed, c). It tablet was used in the photocatalytic activity test.

get a beige powder called 8NC when Phaeozem-soil was used (Figs 1a-b).

The synthesized nanomaterials were characterized by X-ray diffraction (XRD, Smart Lab Rigaku) using the powder configuration, $K\alpha$ radiation of Cu ($\lambda = 1.5406 \text{ \AA}$), and the crystalline phases of the nanomaterials were determined. X-ray diffraction patterns were recorded at 35 kV and 45 mA in the 2θ range of 5° - 80° . The spectral plots were compared with details obtained from the Joint Committee on Powder (JCPDS) for analytical purposes. HR-TEM and STEM (JEOL 2100) were used to analyze the morphology, and HR-TEM revealed lattice spacings for the compounds. The particle size was determined directly from the images by using the software of the equipment Digital Micrograph GatanTM. The chemical composition properties were recorded using a scanning electron microscopy (SEM) and energy dispersive X-ray spectrometer (EDS) (SEM-EDS, Bruker Zeiss). Light absorption was studied using Agilent Ultra Violet-vis diffuse reflectance (UV-vis DRS) spectrophotometer. It has an integrating sphere and a spectral reflectance standard over a wavelength range of 200-800 nm, and the energy gap of nanomaterials composites was determined using the Kubelka-Munck model. Fourier transform infrared (FT-IR) absorption spectra were recorded by a Nicolet 6700 FT-IR instrument. Raman spectra were recorded by NT-MDT INTEGRASpectra using a laser with a 473 nm wavelength as the source and a 600/600 grid. The spectra were traced in the range 3500 - 50 cm^{-1} with 500 scans at 0.1 cm^{-1} resolutions and, the spectral recordings were carried out at room temperature. Both infrared and Raman analysis

permitted the identification of the main molecular groups present in the samples.

The surface compositions of the composites prepared were also analyzed by X-ray photoelectron spectroscopy (XPS) using a Thermo ScientificTM K-AlphaTM+X-ray Photoelectron Spectrometer (XPS) System. The C1s peak calibrated the binding energy at 284.5 eV.

The surface characteristics, the porosity, and the adsorption-desorption isotherms of the material Ag-NP/TiO₂-NP/natural-soil-NP/exhausted coffee-ground produced by the thermal method were studied for a standard volumetric method by nitrogen adsorption at 75 K and the BET equation.

Photocatalytic Activity Test

The photocatalytic performance was constructed on the photocatalytic degradation of the harmful organic pollutant of methylene blue (MB) solutions, under exposure to UV light at room temperature. A tablet of 0.25 g of the composite Ag-NP/TiO₂-NP/Phaeozem natural-soil-NP/ exhausted coffee-ground [Phaeozem soil (8NC)] was put into the quartz cell. Each quartz cell had with 3 mL of an aqueous MB solution at 0, 2.5, 5, and 10 M. The tablet of the composite was removed from the quartz cell during the photocatalytic activity test, and after that, it was put back again until the next determination. The setup was placed in a box sealed with aluminum foil to keep out external light and equipped with a lamp 40 W and wavelength 232 nm. The UV light sources were then turned on, and this moment was considered as time 0 ($t = 0$) for the degradation reaction.

Under room conditions and stirring, the contents of the quartz cell were exposed at regular intervals to UV light for 150 minutes. The obtained solutions were analyzed using a UV-visible spectrophotometer with a quartz cuvette that has an optical length of one cm. The suspension was analyzed following the removal of the photocatalyst. The degradation of the organic pollutant (MB) was determined using a Spectrophotometer Shimadzu Uv-2401 PC. The sample 8NC was placed in the reactor, and the test was carried out for triplicate for each nanomaterial. After regular time intervals of 30 mins, 2 mL of dye solution was sampled, and its concentration was measured by recording the absorbance corresponding to $\lambda \approx 664$ nm for MB.

Antimicrobial Activity

The antimicrobial activity and resistance against *Escherichia coli* and *Staphylococcus aureus* were tested according to EPA (Environmental Protection Agency) by the Antimicrobial Disk Susceptibility method and the Mexican Standard NOM-127-SSA1-1994 [9]. Three sets of simultaneous controls were used. The diameters of the inhibition zones (zone of inhibition-ZOI) were measured in millimeters. The replicates, along with the standard error of the mean (sem), were calculated.

Results and Discussion

Morphological and Structural Characterization

The crystalline structure and crystalline phase composition of the synthesized Ag-NP/TiO₂-NP/natural-soil-NP/exhausted coffee-ground nanomaterial were studied by the X-ray diffraction (XRD). Fig. 2a) shows the X-ray pattern of Phaeozem soils used in the synthesis; diffractions can be assigned to quartz (SiO₂) (Q), kaolinite (K) (Al₂(SiO₂O₅)(OH)₄), mullite (M) (Al₆Si₂O₁₃), among others. The peak located at $2\theta = 28^\circ$, Fig. 2b) (Q), can be assigned to the Phaeozem-soil, which matches with the composite of Ag-NP/TiO₂-NP/Phaeozem-soil-NP/exhausted coffee-ground (8NC). The reflections located at 38.1° , 44.3° , 64.4° and 77.4° (2θ) can be assigned to the (1 1 1), (2 0 0), (2 2 0) and (3 1 1) planes of the cubic phase of Ag with a lattice constant (JCPDS file: 04-0783) from two composites 8NC (Fig. 2c). Therefore, the synthesized material 8NC shows the presence of Ag-NP-TiO₂-NP-soil-NP confirming the composite production, and that is a nanocomposite.

Figs 2d) and 2e) show the crystallinity of the composite before and after it was calcinated. Crystallinity and the crystal phase are crucial parameters that

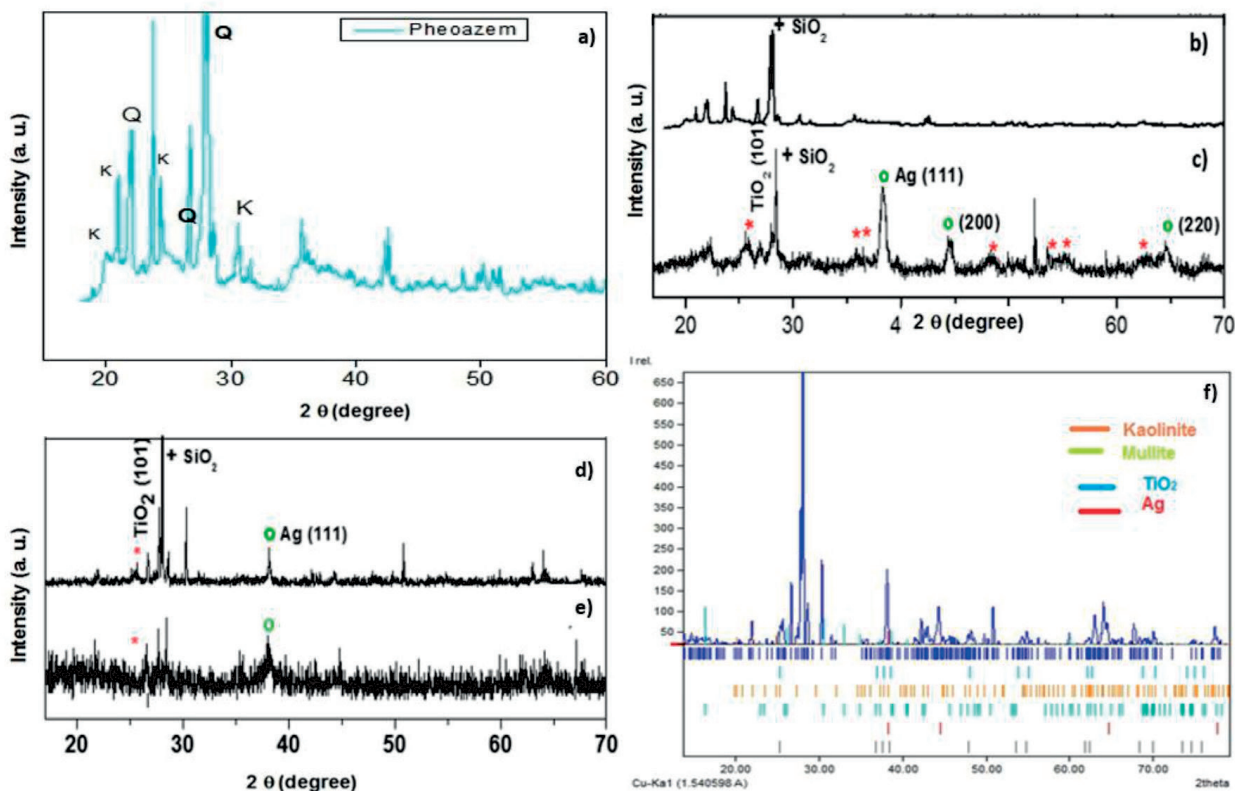


Fig. 2. Characterization of the soil, Ag-nanoparticles, TiO₂-nanoparticles, exhausted coffee ground, and synthesized nanocomposite. a) XRD diffraction patterns of the Phaeozem-soil-NP; b) Diffractogram of Phaeozem soil; c) Diffractogram of the nanomaterial Ag-NP/TiO₂-NP/Phaeozem-soil-NP/exhausted coffee-ground (8NC); d) Nanocomposite Ag-NP/TiO₂-NP/Phaeozem-soil-NP/exhausted coffee-ground (8NC) calcinated; e) Nanocomposite Ag-NP/TiO₂-NP/Phaeozem-soil-NP/exhausted coffee-ground before calcination; f) Phases of calcined 8NC.

determine the photocatalytic activity of TiO_2 . The crystalline anatase phase is considered as the most active form of TiO_2 [10, 11]. The synthesized composites treated with only the thermal method displayed a low crystallinity compared to the treated with the calcination process (Figs 2d, b). It could extend the TiO_2 photoabsorption range from UV to visible light spectrum [12]. Match™ software, with the refinement of the Rietveld method, was used to determine the different phases of the composites. Fig. 2f) shows mullite and kaolinite phases further cubic Ag phase and anatase TiO_2 phase.

The morphology of each sample was observed via an HR-TEM, even when the morphology is not so clear (Fig. 3a), that shows in Ag/ TiO_2 by other authors like a sphere, because composites were synthesized with clays and the nanoparticles of Ag and TiO_2 are into the soil interlayers [13]. The HR-TEM micrographs show the diameter of the Ag nanoparticles in the range of 5-20 nm, TiO_2 nanoparticles is between 15-20 nm in diameter (Fig. 3b), in good agreement with the broadened diffraction peaks of TiO_2 nanoparticles in the X-Ray patterns. The size particle of the natural-soil is not measured, but the size of clays are known with a nanometric size. The size particle was determined directly from the images using the software of the equipment Digital Micrograph Gatan (™). The size

of the particles (Ag-NP, TiO_2 -NP, and soil or clay) of the composite permitted to confirm that it was a nanocomposite.

The micrograph of fast Fourier Transformed (FFT) shows the interplanar crystal spacing of 0.277 nm corresponds to the (2 0 0) plane and the d spacing of 0.236 nm correspond to the (1 1 1) plane of face-centered cubic Ag (Fig. 3c). In contrast, the interplanar crystal spacing of 0.252 nm corresponds to the (1 0 1) plane of anatase TiO_2 phase (Fig. 3d), on red and green, respectively. Other authors showed the interplanar crystal spacing of 0.231 nm for Ag and 0.324 nm for TiO_2 . Still, their composite is $\text{Ag}_2\text{O}/\text{TiO}_2$ on graphene platelets, and for preparation of composite Ag-modified GO- TiO_2 the (1 1 1) plane was found and other d spacing for the different plane (1 0 4) [14]. The selected area of electron diffraction (SAED) pattern indicated that the TiO_2 -NP and clays had good crystallinity (Fig. 3e).

The SEM micrograph of the nanocomposite Ag-NP/ TiO_2 -NP/Phaeozem natural-soil-NP/exhausted coffee-ground was examined (Fig. 3f). On the surface, it can be seen only the natural-soil; for this reason, it cannot check the morphologies and size of the as-synthesized composites and the calcinated composites. The chemical compositions of all synthesized products obtained by the EDS analyses are also presented in

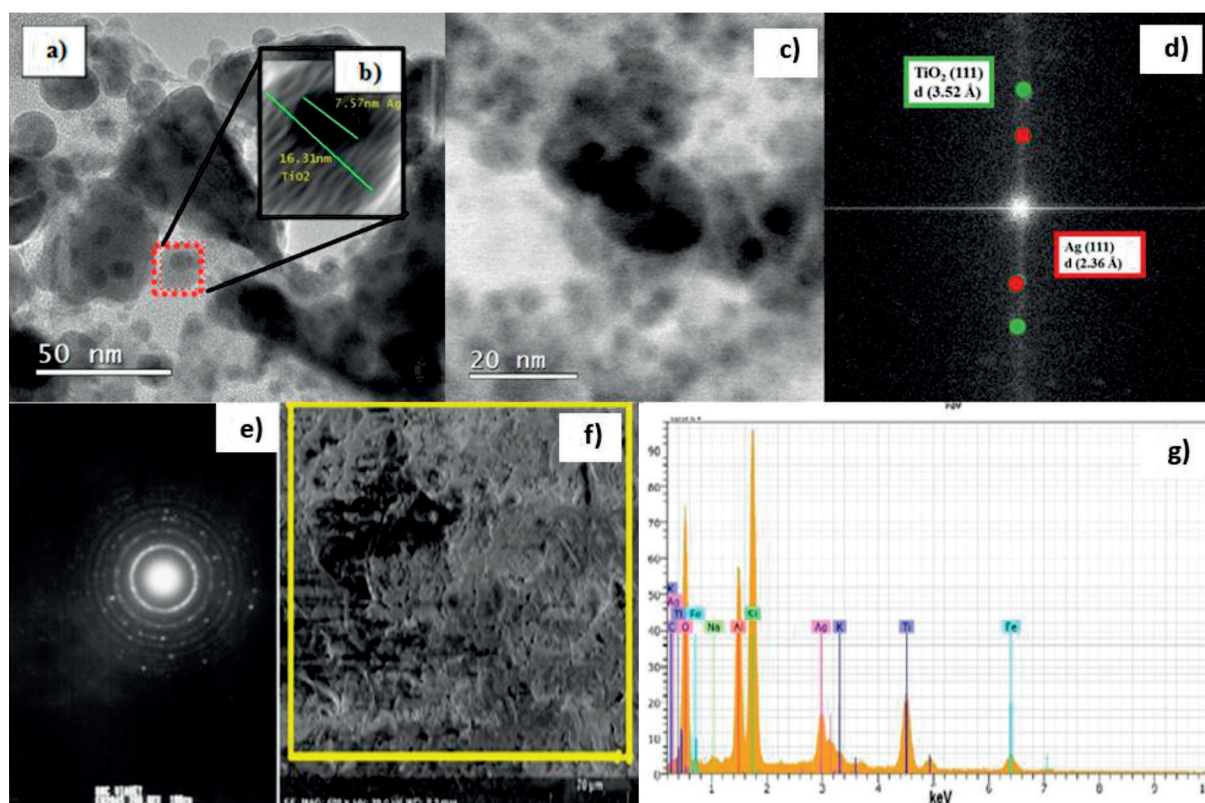


Fig. 3. Electron microscopic characterization of TiO_2 - and Ag- nanoparticles and nanocomposite. HR-TEM micrograph of a) nanocomposites 8NC synthesized-calcinated with Phaeozem-soil and b) diameters of TiO_2 and Ag nanoparticles. STEM micrograph of c) nanocomposite 8NC synthesized-calcinated with Phaeozem-soil and d) FFT lattice of TiO_2 on green and lattice of Ag on red. TEM micrograph of the nanocomposite 8NC synthesized-calcinated with Phaeozem-soil e). SEM micrograph of the nanocomposite 8NC synthesized with Phaeozem-soil f) and SEM-EDS of the nanocomposite 8NC synthesized with Phaeozem-soil g).

Table 1. Properties of the nanocomposite synthesized with Phaeozem-soil.

Properties	Materials			
	Ag-NP	TiO ₂ -NP	Mullita	Kaolinite
Crystalline phase	face-centered-cubic	Anatase		Al ₂ O ₃ Si ₂
Space group	F m -3 m (225)	I 41/a m d (141)	P b a m (55)	C1 c1 (9)
Crystal system	Cubic	Tetragonal	Orthorhombic	Monoclinic
Cell parameters Å	a = 4.088	a = 3.7971 c = 9.5780	a = 7.7391 b = 7.6105 c = 2.9180	a = 51.48 b = 8.92 c = 14.53
d (Å) (hkl) 2θ(°)	2.35(111) 38.1 2.035 (200) 1.22 (220)	3.52(101) 25.94 1.89 (103) 2.39 (004)	5.42 (110) 25.94 2.91 (001) 2.71 (220)	7.15(002)39.61 2.34 (132) 3.57 (004)

Fig. 3g) and show the presence of Si, Al, Ti, and Ag in both composites. These results suggested that silver and TiO₂ were incorporated into the layer of Phaeozem-soil structure by the impregnation and ion exchange. There are other cations like K, Na, and Ca that are part of the soil [15].

Table 1 shows the morphological and structural properties of nanocomposite synthesized with Phaeozem-soil (8NC) obtained by the software mentioned before and confirmed with the JCPDS cards.

UV-vis Absorption Spectra Analysis

The UV-vis DRS of Ag-NP/TiO₂-NP/Phaeozem soil-NP/exhausted coffee-ground (8NC) was obtained at room temperature using an Agilent equipment in the wavelength range of 300-800 nm. An excitation edge at 305 nm and 2.91 eV bandgap for the composite was established (Figs 4a-b), the excitation edges of composites are found to be red-shifted (Fig. 4b). This redshift may be due to the surface plasmon resonance

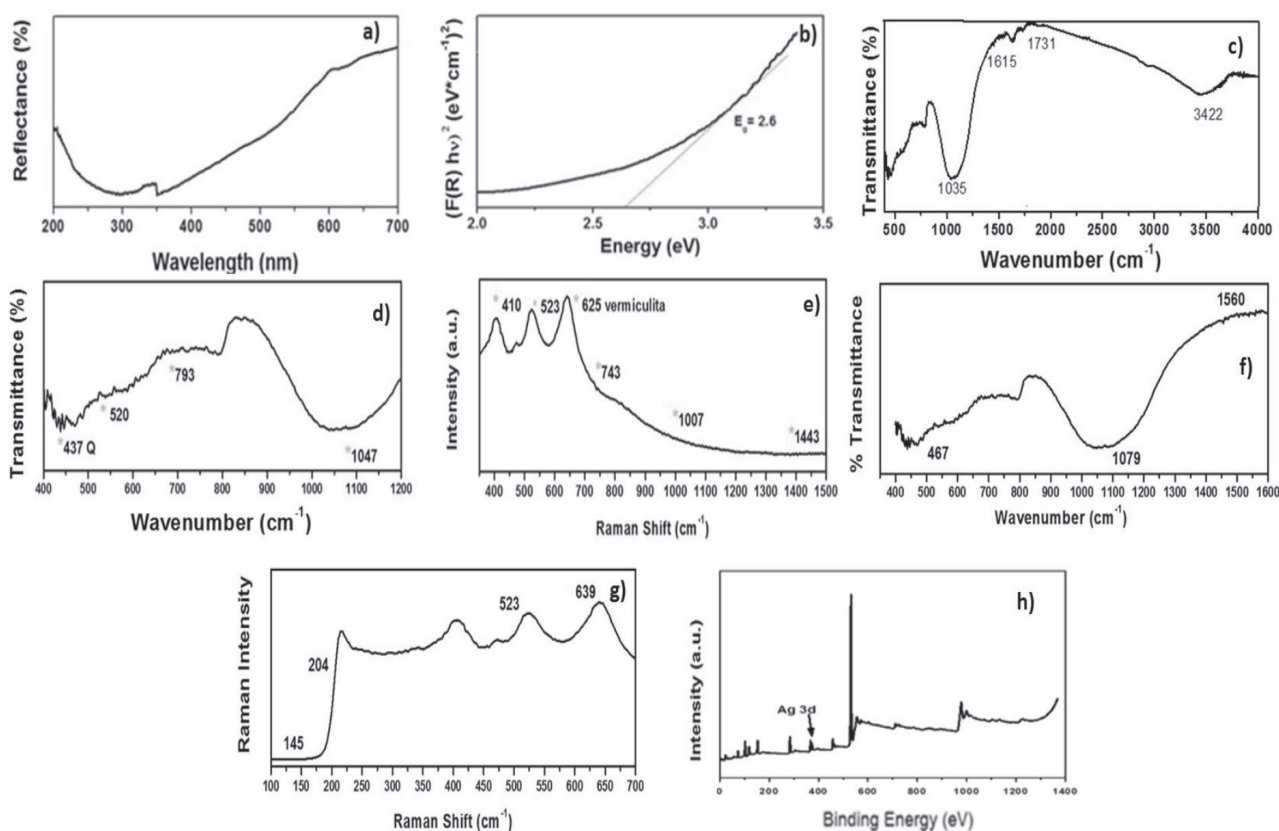


Fig. 4. UV-vis DRS spectra of the 8NC nanocomposites a) and UV-Tauc plot with their respective bandgap energies b). FT-IR spectra c) of the nanocomposite with Phaeozem-soil (8NC). d) FT-IR spectra of SiO₂ nanocomposite 8NC, e) Raman spectra of SiO₂ nanocomposite 8NC, f) FT-IR spectra of TiO₂ of nanocomposite 8NC, g) Raman spectra of TiO₂ nanocomposite, h) XPS spectra of the nanocomposite with Phaeozem-soil (8NC).

(SPR) energy transfer from metal nanoparticles to TiO₂ surface and soil-NP surface and founded when the red line intersects with the curve [15]. The SPR band of composite 8NC appears at 428 nm. The adsorption energies 2.6 eV on composite 8NC surface on their Ag-NP coated by their anatase phase of TiO₂-NP and attached by soil-NP are in the range of 2.9 eV, and the absorption coefficient was $k = 0.8104$. Comparing these results with Ag-NP ($k = 0.059$, bandgap 3.4 eV) and TiO₂-NP ($k = 0.072$, bandgap 3.2 eV), Ag/TiO₂ ($k = 0.145$ band gap = 2.81eV a 500°C) Pt/TiO₂ (bandgap 3.13 eV) [16], and bentonite/TiO₂-NP/AgNP composite reported a 3.05 eV bandgap and $k = 0.017$, k values increased considerably, but band gap values are lower than those reported in literature [16]. The band gaps reduction respect to only TiO₂ (3.2 eV) or Ag/TiO₂ composites can produce superoxide radicals and hydroxyl radicals; these reactive oxidative species enhance the degradation of contaminants of emerging contaminants (ECs). Figs 4a) and 4b) indicate strong interactions between nanoparticles and surfaces. The principal reason of this event is that the interfacial bonds between the interlayer of natural-soil and Ag-NP (1 1 1) and anatase phase TiO₂-NP (1 0 1) permitted a better light absorption ability of 8NC composite.

FT-IR and Raman Analyses

Fig. 4c) shows the FT-IR spectra of materials composites synthesized with Phaeozem-soil (8NC). In Fig. 4c), the 8NC nanocomposite has strong bands related to the presence of bound water (around 3400 cm⁻¹). The water might be bound to hydraulic compounds, like silicate and aluminate hydrates. In Fig. 4c), the band observed at 3500 cm⁻¹, corresponding to the stretching vibration of the hydroxyl group O-H of the TiO₂-NP [16]. The band was found around 1615 cm⁻¹ corresponding to bending modes of water Ti-OH.

The bands at 1040, 799, 525, and 462 cm⁻¹ indicate the presence of silicate phases (Si-O vibrations) when the composites were treated at 500°C. In this work, the bands were found at 1047, 793, 520, and 437 cm⁻¹ (Fig. 4d). Furthermore, the spectra of FT-IR the crystalline β quartz exhibit the primary band at 1042 cm⁻¹ corresponding to antisymmetric Si O Si stretching vibration, as witnessed in Fig. 4d) for composite 8NC. In the 8NC nanocomposite, there is another band at 625 cm⁻¹ at the spectrum, corresponding to the stretching vibration of the vermiculite [17] (Fig. 4e).

Fig. 4f) shows the bands at 1560, 1079, and 467 cm⁻¹ correspondings to the TiO₂ phase anatase. Fig. 4g) shows the Raman spectrum for the 8NC nanocomposite. It presented different Raman active modes with the monoclinic TiO₂ phase with the C2/m group. The bands observed between 400 to 600 cm⁻¹ that should be corresponding to Ti-O modes (Eg(1), Eg(2), Eg(3), and Ag(1)) at 143, 637, 196 and 514 cm⁻¹ respectively in Raman spectra [17]. However, in this research, bands were observed at 145, 639, 204 and 523 cm⁻¹.

XPS Analysis

XPS analyses of the silver, titanium, oxygen, and silicon-containing in composite synthesized using a Phaeozem-soil (8NC) as the titanium source and silver source were carried out to determine the surface composition and oxidation states of the active metals (Fig. 4h).

The XPS Ag 3d spectrum of those composites exhibit the binding energy of Ag 3d5/2 line at 367.08 eV to composite 8NC with Phaeozem-soil that is characteristic of Ag with oxidation state (0). It is in agreement with the kinetic energy of the Ag M5N45N45 Auger peak at 357.7 eV [18]. Fig. 5a) shows that the nanomaterial with Phaeozem-soil exhibits the binding energy of the Ag 3d5/2 line at 367.08 eV.

Natural soil (Phaeozem) and exhausted coffee ground mixed with ethanol contain vast numbers of hydroxyl groups that can act as good chemical reductants. The presence of this functional group in the synthesis process facilitates the formation of metal nanoparticles. The sequestration of cations [Mn⁺] or hydroxylated cations [M(OH)]^{m+} that can endure nucleation or growth processes is accelerated by the highly reactive hydroxyl groups present in natural-soil and coffee ground. After the hydrothermal process, when 8NC was calcinated at 500 °C, it formed the TiO₂-NP anatase phase. It raised the formation of dispersed oxides (Fig. 5a, 5b, and 5c), while the oxidations states of Ag 3d was present, and the oxidation states of Ti was 4+. In Fig. 5c) centers formed creating shallow and deep trap states, which contributed to the reduction of the bandgap and inducing separation of photo-induced charge pairs, the electrons, and the holes are present in the nanocomposite 8NC; it permitted the enhancement on catalyst activity [19].

The presence of Ag 3d (Fig. 5a) allowed confirming the antimicrobial activity of the composite 8NC, and the formation of the Schottky barrier is only possible when silver transition metal is present in its elemental state (0) which has been confirmed by XPS analysis. It will enhance its catalyst activity and, consequently, its antimicrobial activity.

Antimicrobial Activity of the Nanocomposite Ag-NP/TiO₂-NP/natural-soil-NP/exhausted Coffee-Ground

Screening for antimicrobial activity by the Disk Diffusion Method, which is based on the principle that each of the live bacteria can grow into a colony, was carried out. The antimicrobial activity is evidenced by an inhibition zone of bacteria *E. coli* and bacteria *S. aureus* growth around the composite (Figs 5d and 5e). No bacterial growth was observed on the top of and adjacent to the nanomaterial composite for Ag-NP/TiO₂-NP/Phaeozem natural-soil-NP/exhausted coffee ground. The result demonstrates that the composite could inhibit bacterial growth. The time-dependent durability of the

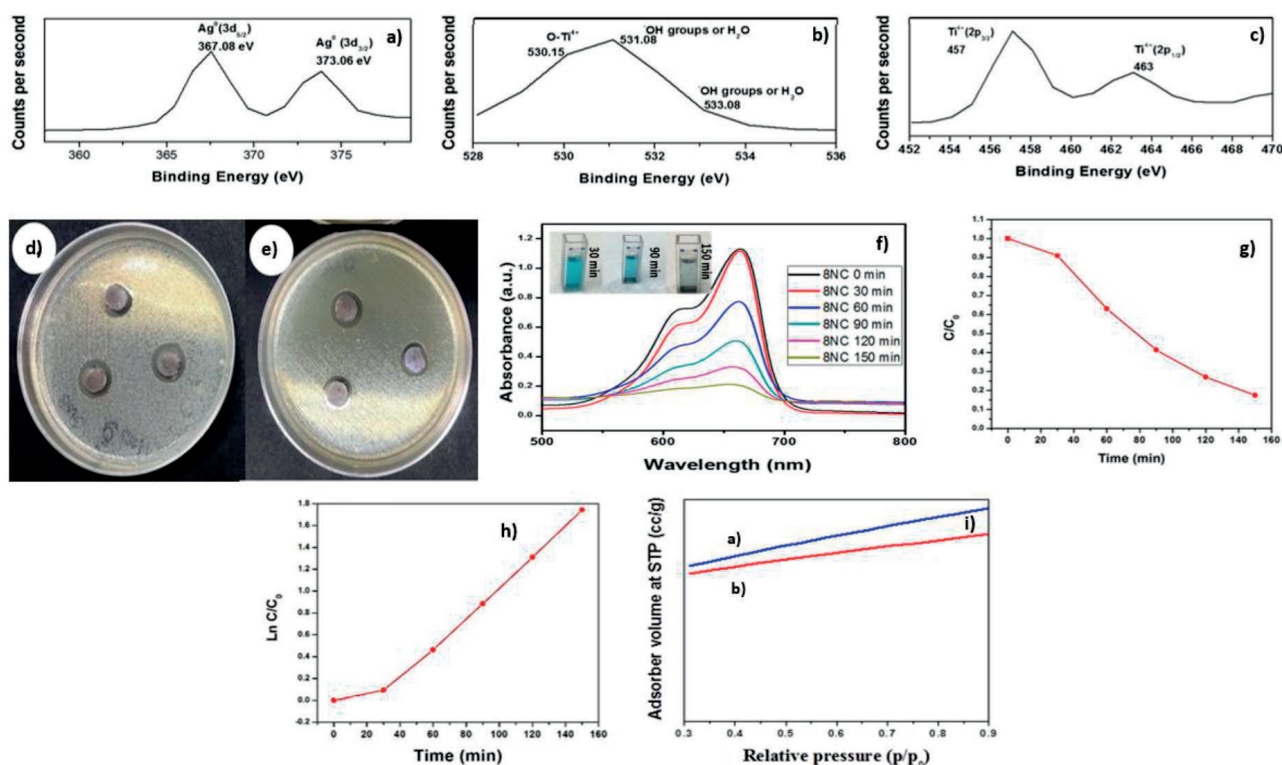


Fig. 5. High-resolution XPS spectra of a) Ag 3d of the nanocomposite with Phaeozem-soil (8NC), b) O 1s of the nanocomposite with Phaeozem-soil, and c) Ti 2p of the nanocomposite with Phaeozem-soil. Antimicrobial activity of the synthesized nanocomposite with Phaeozem-soil 8NC against d) *E. coli*, and e) against *S. aureus*. f) variation in methylene blue dye concentration with sunlight irradiation time in the presence of Ag-NP/TiO₂-NP/Phaeozem-soil-NP/exhausted coffee-ground (8NC). (g and h) Kinetics of decomposition of methylene blue by the photocatalysts of the nanocomposite 8NC. j) Isotherm graph of a Phaeozem soil a) and of Nanocomposite 8NC b).

synthesized composite was also studied for different time intervals, and the diameter of inhibition of nanocomposite 8NC was 15(0.0) mm in two bacteria. It was found that Ag-NP/TiO₂-NP/Phaeozem-soil-NP/exhausted coffee-ground has functional inhibition and bacterium suppression. Other authors presented ZOI = 25 mm for the composite of Ag deposited into TiO₂-NP [20], or a ZOI of 4 mm for the composite Ag collected on MMT for *S. aureus* and is not able for inhibition of *E. coli* [21]. The effect that hydrophilic OH groups are created on illuminated via UV light irradiation TiO₂ surface is well known [22]. The loading of silver does not affect the photoinduced hydrophilicity of TiO₂, but the result reveals that the composite inhibited bacterial growth (Figs 5d-e). The high antimicrobial activity of the composites under the UV light is due to the synergistic antimicrobial effects of the photocatalytic reaction of the TiO₂ coating and silver.

The effect in which are created hydrophilic OH groups on illuminated via UV light irradiation TiO₂ surface is well known [22]. The loading of silver does not affect the photoinduced hydrophilicity of TiO₂, but the result reveals that two composites could inhibit bacterial growth (Figs 5d-e). The high antimicrobial activity of the composites under the UV light is due to the synergistic antimicrobial effects of the photocatalytic reaction of the TiO₂ coating and silver.

The enhanced antimicrobial activity of irradiated composites is attributed to the production of reactive oxygen species (ROS) by the release of metal ions (Ag⁺ in this work), which are produced by the presence of Ag₃d. The formation of the Schottky barrier is only possible when metal is present in its elemental state, which has been confirmed from XPS analysis; this permitted the enhancement of catalyst activity [23].

Photocatalytic of Nanocomposites Synthesized with Phaeozem-soil on MB Degradation

The degradation reaction kinetics of the dyes with and without photocatalyst was monitored by collecting UV/Vis spectra after a regular interval of times (30 minutes). Fig. 5f) shows a series of absorbance spectra of MB with initial concentration using composite 8NC as a photocatalyst, respectively. The graphics show the range of 500 to 800 nm, and the two major absorption peaks appear at $\lambda = 612$ and 664 nm, which are characteristic of MB. When it is exposed to UV light, the absorbance reduced with increasing exposure time and dye degradation identified by color change, indicating photocatalytic activity of the composites 8NC. In this experiment, the pH of the solution was not controlled. However, the maximum adsorption of malachite green was obtained at an optimum pH of 7,

when trisodium citrate-based magnetite nanocomposite was used [24].

Comparing the photocatalytic and absorbance performance of the composites 8NC on MB degradation, it was demonstrated that the nanocomposite 8NC had an excellent photocatalytic activity. It has been reported that at a greater surface area, the photocatalysis increases. In this evaluation, the nanocomposite 8NC (Fig. 5f) shows the degradation of organic MB pollutants. The surface area of this nanocomposite was $45 \text{ m}^2\text{g}^{-1}$.

Figs 5g) shows the kinetics analysis of reactions in and 8NC. The photocatalytic degradation of MB dye was 82.31 % by 150 minutes. It was because the Phaeozem-soil has a high surface area, and it allowed that a higher number of active sites on the photocatalyst surface became available. So, the quantity of -OH radicals that were produced could have had more significant interaction and facilitated their participation in the dye degradation process. 8NC did not degrade enough MB compared to other materials with carbon dots, Ag, and TiO_2 -NP with the commercial name P25. P25 exhibited a photocatalytic performance in MB degradation of 100% by 15 min, under UV light [25], even when reported a surface area of $62.5 \text{ m}^2 \text{ g}^{-1}$. However, the maximum degradation (28%) of MB was observed at 50 ppm when gum arabic-crosslinked-poly (acrylamide)/Ni(OH)₂/FeOOH nanocomposites hydrogel was used [25].

The photocatalytic kinetics (Fig. 5h) was studied using the Langmuir-Hinshelwood equation for calculating the rate constant of degradation of MB, k (min^{-1}) under UV light. The value of the rate constant for the nanocomposite was 0.0116 min^{-1} due, among other things, to its large surface area ($31.48 \text{ m}^2 \text{ g}^{-1}$) [26]. Another experimental data revealed that the adsorption of MB dye by 2-amino-5-guanidinopentanoic acid modified activated carbon (AGDPA@AC) was followed by Langmuir isotherm well with a maximum adsorption capacity of 219.9 mg/g [3].

To investigate the adsorption mechanism, the models of pseudo-first order and pseudo-second order were applied by [3]. In that study, thermodynamic results showed that the adsorption of MB was spontaneous and exothermic nature. The reusability of AGDPA@AC showed that after even four cycles, the adsorption percent was 75%, which indicated that AGDPA@AC is a probable renewable adsorbent. According to [3], MB could be attached to functional groups viz, carboxylic, amino, and amido groups. So, the adsorption occurred by two mechanisms: electrostatic interaction between electron-rich oxygen and nitrogen and π - π interaction between the surface of AGDPA@AC and MB dye. In this research, similar adsorption mechanisms could be present as witnessed by FT-IR and Raman analyses because there are electron-rich oxygen and N, and hydroxyl groups. The last group has a valence charge of -1, while the MB dye has a positive charge (+1).

Nitrogen-Adsorption Isotherms, Surface Areas, and Pore Volumes

The surface area of the nanocomposite was $31.48 \text{ m}^2\text{g}^{-1}$. Still, some works reported that TiO_2 -NP had a surface area of $42.6 \text{ m}^2\text{g}^{-1}$ with a lower photocatalytic [27]. All isotherms of adsorption and desorption curves for the soil and nanomaterials synthesized show a type III isotherm and hysteresis loops typical a microporous material (Fig. 5i). The nanocomposite synthesized with Phaeozem soil (8NC) had a larger surface area and photo-generated electrons and holes. The electron reacts with O_2 to produce O_2^- and increases and improves the photocatalytic activity.

Conclusions

Clays from a Phaeozem soil were used to synthesis a nanocomposite with Ag- and TiO_2 - nanoparticles and exhausted coffee ground. The nanocomposite was fully characterized by cutting-edge scientific equipment, and according to the results, it can degrade the organic pollutant methylene blue. Also, the nanocomposite has antimicrobial activity and could dissipate other harmful chemicals. Besides, this nanocomposite can also be used to chelate and separate other contaminants from soil or water, as witnessed by FT-IR and RAMAN characterization.

Acknowledgments

This research was funded by 'Ciencia Básica SEP-CONACyT' project 287225, 'Fondo FONCYT-COECYT-Convocatoria 2019-C13, Efecto de Nanopartículas de Uso Agrícola Sobre el Desarrollo de la Planta de Maíz (*Zea mays* L.) y las Propiedades Físicoquímicas y Biológicas del Suelo (COAH-2019-C13-C006)', CONACyT-SINANOTOX PN-2017-01-4710, the Sustainability of Natural Resources and Energy Programs (Cinvestav-Salttillo), and Cinvestav Zacatenco. Urdapilleta-Inchaurregui is grateful for postgraduate fellowship through CONACyT as well as for CINESTAV-IPN. Special thanks for D. Bahena, J. Roque, M. Guerrero Fuentes for their technical support (STEM, SEM, and XRD analyses).

Conflict of Interest

The authors declare no conflict of interest.

References

1. TARA N., SIDDIQUI S.I., RATHI G., CHAUDHRY S.A., INAMUDDIN, ASIRI A.M. Nano-engineered adsorbent for the removal of dyes from water: a review. *Curr. Anal. Chem.*, **16** (1), 14, 2020.

2. KEULEMANS M., VERBRUGGEN S.W., HAUCHECORNE B., MARTENS J.A., LENAERTS S. Activity versus selectivity in photocatalysis: Morphological or electronic properties tipping the scale. *J. Catal.*, **334**, 221, **2016**.
3. NAUSHAD M., ALQADAMI A.A., ALOTHMAN Z.A., ALSOHAIMI I.H., ALGAMDI M.S., ALDAWSARI A.M. Adsorption kinetics, isotherm and reusability studies for the removal of cationic dye from aqueous medium using arginine modified activated carbon. *J. Mol. Liq.*, **293**, Article number UNSP111442, **2019**.
4. NAUSHAD M., ALOTHMAN Z.A., AWUAL M.R., ALFADUL S.M., AHAMAD T. Adsorption of rose Bengal dye from aqueous solution by amberlite Ira-938 resin: kinetics, isotherms, and thermodynamic studies, *Desalin. Water Treat.*, **57**, 29, 13527, **2016**.
5. XU T.Z., ZHAO H.C., ZHENG H., ZHANG P.Y. Atomically Pt implanted nanoporous TiO₂ film for photocatalytic degradation of trace organic pollutants in water. *Chem. Engin. J.*, **385**, 123832, **2020**.
6. GARCÍA-ZALETA D.S., TORRES-HUERTA A.M., DOMINGUEZ-CRESPO M.A., GARCÍA-MURILLO A., SILVA-RODRIGO R., GONZALEZ R.L. Influence of phases content on Pt/TiO₂, Pd/TiO₂ catalysts for degradation of 4-chlorophenol at room temperature. *J. Nanomater.*, 1805169, **2016**.
7. KHAN I., SAEED K., KHAN I. Nanoparticles: Properties, applications and toxicities. *Arab. J. Chem.*, **12** (7), 908, **2019**.
8. UNUABONAH E.I., UGWUJA C.G., OMOROGIE M.O., ADEWUYI A., OLADOJA N.E. Clays for efficient disinfection of bacteria in water. *Appl. Clay Sci.*, **151**, 211, **2018**.
9. HUMPHRIES R.M., KIRCHER S., FERRELL A., KRAUSE K.M., MALHERBE R., HSIUNG A., BURNHAM C.A.D. The continued value of disk diffusion for assessing antimicrobial susceptibility in clinical laboratories: Report from the clinical and laboratory standards institute methods development and standardization working group. *J. Clin. Microb.*, **56**, 8, UNSPe00437-18, **2018**.
10. YU X., SHANG L.W., WANG D.J., AN L., LI Z.H., LIU J.W., SHEN J. Plasmon-resonance-enhanced visible-light photocatalytic activity of Ag quantum dots/TiO₂ microspheres for methyl orange degradation. *Solid State Sci.* **80**, 1, **2018**.
11. YAN W.Y., ZHOU Q., CHEN X., YANG Y., ZHANG Y., HUANG X.J., WU Y.C. Size-Controlled TiO₂ nanocrystals with exposed {001} and {101} facets strongly linking to graphene oxide via p-Phenylenediamine for efficient photocatalytic degradation of fulvic acids. *J. Hazard. Mater.* **314**, 41, **2016**.
12. ZHANG Y., WANG T., ZHOU M., WANG Y., ZHANG Z.M. Hydrothermal preparation of Ag-TiO₂ nanostructures with exposed {001}/{101} facets for enhancing visible light photocatalytic activity. *Ceram. Int.* **43** (3), 3118, **2017**.
13. MAKAL P., DAS D. Self-doped TiO₂ nanowires in TiO₂-B single phase, TiO₂-B/anatase and TiO₂-anatase/rutile heterojunctions demonstrating individual superiority in photocatalytic activity under visible and UV light. *Appl. Surf. Sci.* **455**, 1106, **2018**.
14. QI H.P., WANG H.L., ZHAO D.Y., JIANG W.F. Preparation and photocatalytic activity of Ag-modified GO-TiO₂ mesocrystals under visible light irradiation. *Appl. Surf. Sci.* **480**, 105, **2019**.
15. TOMUL F., BASOGLU F.T., CANBAY H. Determination of adsorptive and catalytic properties of copper, silver and iron contain titanium-pillared bentonite for the removal bisphenol A from aqueous solution. *Appl. Surf. Sci.* **360**, 579, **2016**.
16. MARTINS R.C., DOMINGUES E., BOSIO M., QUINA M.J., GMUREK M., QUINTA-FERREIRA R.M., GOMES J. Effect of different radiation sources and noble metal doped onto TiO₂ for contaminants of emerging concern removal. *Water*, **11** (5), 894, **2019**.
17. FISCHER C.E., MINK J., HAIBA L., BACSIK Z., NEMETH C., MIHALI J., RAITH A., COKOJA M., KUHN F.E. Vibrational spectroscopic study of SiO₂-based nanotubes. *Vib. Spectrosc.* **66**, 104, **2013**.
18. MIKHLIN Y.L., VOROBYEV S.A., SAIKOVA S.V., VISHNYAKOVA E.A., ROMANCHENKO A.S., ZHARKOV S.M., LARICHEV Y.V. On the nature of citrate-derived surface species on Ag nanoparticles: Insights from X-ray photoelectron spectroscopy. *Appl. Surf. Sci.* **427**, 687, **2018**.
19. MISHRA A., MEHTA A., KAINTH S., BASU S. Effect of different plasmonic metals on photocatalytic degradation of volatile organic compounds (VOCs) by bentonite/M-TiO₂ nanocomposites under UV/visible light. *Appl. Clay Sci.* **153**, 144, **2018**.
20. WILKE C.M., WUNDERLICH B., GAILLARD J.F., GRAY K.A. Synergistic bacterial stress results from exposure to nano-Ag and nano-TiO₂ mixtures under light in environmental media. *Environ. Sci. Tech.* **52** (5), 3185, **2018**.
21. BONGA D.L.S., PINTO M.M.F.B., TAYAD M.F.T. Synthesis and characterization of silver nanoparticles anchored on montmorillonite via chemical reduction. *Int. J. Sci. Eng. Res.* **11**, 30, **2016**.
22. SINGH J., SAHU K., MOHAPATRA S. Thermal annealing induced evolution of morphological, structural, optical and photocatalytic properties of Ag-TiO₂ nanocomposite thin films. *J. Phys. Chem. Solids*, **129**, 317, **2019**.
23. KHAN M.R., CHUAN T.W., YOUSUF A., CHOWDHURY M.N.K., CHENG C.K. Schottky barrier and surface plasmonic resonance phenomena towards the photocatalytic reaction: study of their mechanisms to enhance photocatalytic activity. *Catal. Sci. Technol.* **5** (5), 2522, **2015**.
24. ALQADAMI A.A., NAUSHAD M., ABDALLA M.A., KHAN M.R., ALOTHMAN Z.A. Adsorptive removal of toxic dye using Fe₃O₄-TSC nanocomposite: Equilibrium, kinetic, and thermodynamic studies. *J. Chem. Engin. Data.* **61**, 3806, **2016**.
25. NAUSHAD M., SHARMA G., ALOTHMAN Z.A. Photodegradation of toxic dye using gum arabic-crosslinked-poly(acrylamide)/Ni(OH)₂/FeOOH nanocomposites hydrogel. *J. Cleaner Product.*, **241**, UNSP118263, **2019**.
26. WANG C.L., YANG K., WEI X.H., DING S., TIAN F., LI F. One-pot solvothermal synthesis of carbon dots/Ag nanoparticles/TiO₂ nanocomposites with enhanced photocatalytic performance. *Ceram. Int.* **44** (18), 22481, **2018**.
27. SARANYA K.S., PADIL V.V.T., SENAN C., PILANKATTA R., SARANYA K., GEORGE B., WACLAWEK S., CERNIK M. Green synthesis of high temperature stable anatase titanium dioxide nanoparticles using gum kondagogu: characterization and solar driven photocatalytic degradation of organic dye. *Nanomaterials.* **8** (12), 1002, **2018**.